Dasatinib Is an Effective Treatment for Angioimmunoblastic T-cell Lymphoma

Tran B. Nguyen[1], Mamiko Sakata-Yanagimoto[1,2], Manabu Fujisawa[3], Sharna Tanzima Nuhat[3], Hiroaki Miyoshi[4], Yasuhito Nannya[5], Koichi Hashimoto[6], Kota Fukumoto[3], Olivier A. Bernard[7], Yusuke Kiyoki[2], Kantaro Ishitsuka[2], Haruka Momose[2], Shinichiro Sukegawa[2], Atsushi Shinagawa[8], Takuya Suyama[8], Yuji Sato[9], Hidekazu Nishikii[1,2], Naoshi Obara[1,2], Manabu Kusakabe[1,2], Shintaro Yanagimoto[10], Seishi Ogawa[5], Koichi Ohshima[4], and Shigeru Chiba[1,2,11]

ABSTRACT

Recurrent hotspot (p.Gly17Val) mutations in *RHOA* encoding a small GTPase, together with loss-of-function mutations in *TET2* encoding an epigenetic regulator, are genetic hallmarks of angioimmunoblastic T-cell lymphoma (AITL). Mice expressing the p.Gly17Val RHOA mutant on a *Tet2*-null background succumbed to AITL-like T-cell lymphomas due to deregulated T-cell receptor (TCR) signaling. Using these mice to investigate therapeutics for AITL, we found that dasatinib, a multikinase inhibitor prolonged their survival through inhibition of hyperactivated TCR signaling. A phase I clinical trial study of dasatinib monotherapy in 5 patients with relapsed/refractory AITL was performed. Dasatinib was started at a dose of 100 mg/body once a day and continued until days 10–78 (median day 58). All the evaluable patients achieved partial responses. Our findings suggest that AITL is highly dependent on TCR signaling and that dasatinib could be a promising candidate drug for AITL treatment.

Significance: Deregulated T-cell receptor signaling is a critical molecular event in angioimmunoblastic T-cell lymphoma and can be targeted with dasatinib.

Introduction

Angioimmunoblastic T-cell lymphoma (AITL) is among the most devastating cancers with a 5-year survival of 30% (1–3). AITL comprises 20% of peripheral T-cell lymphomas (PTCL) and is the second most common PTCL subtype (1). Most patients with AITL exhibit symptoms suggestive of immune activation, such as high fever, skin rash, and autoimmune-like conditions. Moreover, AITL tumor cells display features of T follicular helper (T_{FH}) cells, expressing CD4, programmed death-1 (PD1), inducible co-stimulator (ICOS), C-X-C motif chemokine ligand 13 (CXCL13), C-X-C chemokine receptor type 5 (CXCR5), and B-cell lymphoma 6 (BCL6; ref. 4). A variety of immune cells, such as B immunoblasts and eosinophils, massively infiltrate into AITL tissues.

Genomic studies have identified recurrent mutations in *Ras homolog gene family, member A (RHOA)* in 50%–70% of AITL samples (5–7). *RHOA* mutations occur almost exclusively at the p.Gly17Val hotspot, designated G17V. Notably, a substantial proportion (47%–83%) of AITL samples also exhibits loss-of-function mutations in *Ten-Eleven Translocation-2* (*TET2*), which encodes an epigenetic regulator modifying a DNA cytosine methyl group (5, 6, 8). Mutations in both genes overlap in up to 70% of AITL cases (5).

RHOA encodes a small GTPase found in either active GTP-bound or inactive GDP-bound forms, a status controlled by the coordinated action of guanine exchange factors (GEF; for activation) and GTPase-activating proteins (GAP; for inactivation; ref. 9). The G17V RHOA–mutant fails to transmit RHOA signaling; instead, it acquires a neo-function to take VAV1 as a binding partner (10). VAV1, a GEF that also contains Src homology (SH) domains, plays key roles in GEF-dependent and -independent manners (11). G17V RHOA binding to VAV1 increases its phosphorylation. This may trigger phosphorylation of phospholipase C gamma 1 (PLCγ1) and transcriptional activity of nuclear factor of activated T-cell, consequently leading to the enhancement of T-cell receptor (TCR) signaling *in vitro* (10).

Here, we provide *in vivo* evidence showing the G17V RHOA–VAV1–TCR axis and its suppression by dasatinib, a multikinase inhibitor, in a mouse AITL model–expressing G17V RHOA mutant in the context of *Tet2* deletion. Consequently, dasatinib successfully suppressed disease progression in these mice. Moreover, a clinical trial involving patients with relapsed/refractory AITL implied a high response rate to dasatinib treatment.

[1]Department of Hematology, Faculty of Medicine, University of Tsukuba, Tsukuba, Ibaraki, Japan. [2]Department of Hematology, University of Tsukuba Hospital, Tsukuba, Ibaraki, Japan. [3]Department of Hematology, Graduate School of Comprehensive Human Sciences, University of Tsukuba, Tsukuba, Ibaraki, Japan. [4]Department of Pathology, School of Medicine, Kurume University, Kurume, Fukuoka, Japan. [5]Department of Pathology and Tumor Biology, Graduate School of Medicine, Kyoto University, Sakyo-ku, Kyoto, Japan. [6]Tsukuba Clinical Research and Development Organization, University of Tsukuba, Tsukuba, Ibaraki, Japan. [7]INSERM U1170, Gustave Roussy, Université Paris-Saclay, Equipe Labellisée Ligue Nationale Contre le Cancer, Villejuif, France. [8]Department of Hematology, Hitachi General Hospital, Hitachi, Ibaraki, Japan. [9]Department of Hematology, Tsukuba Memorial Hospital, Tsukuba, Ibaraki, Japan. [10]Division for Health Service Promotion, University of Tokyo, Bunkyo-ku, Tokyo, Japan. [11]Life Science Center for Survival Dynamics, Tsukuba Advanced Research Alliance, University of Tsukuba, Tsukuba, Ibaraki, Japan.

Note: Supplementary data for this article are available at Cancer Research Online (http://cancerres.aacrjournals.org/).

T.B. Nguyen and M. Sakata-Yanagimoto contributed equally to this article.

Corresponding Authors: Shigeru Chiba, University of Tsukuba, 1-1-1 Tennodai, Tsukuba, Ibaraki 305-8575, Japan. Phone: 812-9853-3103; Fax: 812-9853-8079; E-mail: schiba-tky@umin.net; and Mamiko Sakata-Yanagimoto, sakatama-tky@umin.net

Cancer Res 2020;80:1875–84

doi: 10.1158/0008-5472.CAN-19-2787

Materials and Methods

Mice

A cDNA encoding the human G17V *RHOA* transgene was inserted into a VA *CD2* transgene cassette containing the upstream gene regulatory region and locus control region of the human *CD2* gene (12). This construct was injected into C57BL/6 fertilized eggs to generate transgenic mice. The G17V *RHOA* transgenic mice were genotyped via PCR using a specific pair of primers (Supplementary Table S1). *Tet2*$^{flox/flox}$ (13) mice have been described previously. *Mx-Cre* mice (14) were purchased from CLEA Japan, Inc.. *Mx-Cre* mice were mated with *Tet2*$^{flox/flox}$ and G17V *RHOA* transgenic mice to get *Mx-Cre* x *Tet2*$^{flox/flox}$ x G17V *RHOA* transgenic mice. Polyinosinic: polycytidylic (pIpC) was peritoneally injected to all 3- to 4-week-old mice at a dose of 20 mg/kg of body weight every other day with 4 doses in total. In *Mx-Cre* with *Tet2*$^{flox/flox}$ mice, exons 10-11 of *Tet2* were deleted and *Tet2*-null mice were generated. Four genotypes of mice, including *Tet2*$^{flox/flox}$ [used as wild-type (WT) control], *Tet2*-null, *Tet2*$^{flox/flox}$ mice crossed with G17V *RHOA* transgenic mice (G17VRHOA), and *Tet2*-null G17VRHOA (Tet2$^{-/-}$G17VRHOA), were followed up. In all experiments, WT and Tet2$^{-/-}$G17VRHOA mice were analyzed at the same age.

The study was approved by the Institutional Review Board at the Laboratory Animal Resource Center of the University of Tsukuba (Tsukuba, Ibaraki, Japan). Mice were maintained in specific pathogen-free conditions. All experiments were performed according to the guidelines of the Laboratory Animal Resource Center.

Flow cytometric analysis

Mouse spleens and lymph nodes were minced and passed through 70 μm Cell Strainer (Falcon) to make single-cell suspensions. The single-cell suspensions of spleens and lymph nodes were lysed with ammonium-chloride-potassium buffer to eliminate red blood cells. Multicolor flow cytometric analysis was performed on BD FACS Aria II (BD Biosciences) and the obtained data were analyzed by the FlowJo software (BD Biosciences). The used antibodies were listed in Supplementary Table S2.

Histologic and immunofluorescence staining of mouse tissue

Parts of organs were fixed with 10% formalin in 0.01 mol/L phosphate buffer (pH 7.2) and embedded in paraffin. Sections were stained with hematoxylin and eosin for histopathologic examination and photographed using a Keyence BZ X710 microscope (Keyence Corporation). Other parts of organs were fixed in 4% paraformaldehyde for 5 hours at 4°C, and then stocked in OCT Compound (Sakura Finetek Japan Co.) at −80°C. The OCT blocks were sliced into 5-μm sections. The sections were incubated with primary antibodies (Supplementary Table S2) against mouse-PD1 (1:50), -CD4 (1:500), -ICOS (1:100), -phosphoVav1 Tyr-174 (pVav1, 1:100), and pPLCγ1 (1:50) for 90 minutes at room temperature. All secondary antibodies listed in Supplementary Table S2 were diluted at 1:1,000 and incubated with the sections at room temperature for 30 minutes. After incubation with DAPI (Vectashield Mounting Medium; Vector laboratories), the stained samples were photographed using a Leica TCS SP5 Confocal Laser Scanning Microscope (Leica Microsystems).

Cytokine analysis

Mouse plasma was collected and stored at −80°C. Cytokines in mouse plasma including IL2, IL4, IL6, IL10, IL17A, IL21, TNF, and IFNγ were analyzed using BD Cytometric Bead Assay Flex Set Kit (BD Life Sciences) according to the manufacturer's protocol.

RNA sequencing

Mouse CD4^{+} splenocytes from tumor-bearing Tet2$^{-/-}$G17VRHOA mice ($n = 3$) and WT mice ($n = 4$) at the same age were isolated using BD FACS Aria II (BD Biosciences). RNA was extracted with RNeasy Mini Kit (Qiagen) and DNase I (BD Biosciences). Illumina sequencing libraries were made from 150 ng of total RNA by TrueSeq RNA Sample Preparation v2 LS Kit (Illumina) following the manufacturer's protocol. Libraries were validated using Bioanalyzer (Agilent Technologies) to determine size distribution and concentration. Sequencing was performed at Tsukuba i-Laboratory LLP (Ibaraki, Japan) using NextSeq500 (Illumina) with a paired-end 36-base read option. Sequencing reads were mapped on the mm10 mouse reference genome and quantified using CLC Genomics Workbench version 9.5.1 (Qiagen). Fragments per kilo base of transcript per million mapped reads (FPKM) values were estimated for each gene and filtered by Empirical Analysis of Digital Gene Expression tool. Gene set enrichment analysis was done by GSEA ver. 2.0 (15). Gene sets of normalized enrichment score were listed on the basis of FDR q value (<0.25) and *P* value (<0.05). The data were deposited in GEO with accession number as GSE144654.

Mouse tumor transplantation

Approximate 2×10^7 cells of single-cell suspension prepared from whole swollen lymph nodes were intraperitoneally injected into 5-week-old BALB/c *nu/nu* (nude) mice (Charles River Laboratory) with or without irradiation. In the irradiation protocol, mice were irradiated with 2 Gy before the injection. Mice were weighted every day and tumor engraftment was checked in peripheral blood at days 7 and 14 after transplantation. Successful engraftment was defined as the percentage of donor H2Kb (MHC class I alloantigen of C57BL/6 mice)-positive cells higher than 0.01% in peripheral blood.

Protocol for mouse treatment

After the single-cell suspension of whole lymph nodes was intraperitoneally injected into nonirradiated nude mice, dasatinib (Cayman Chemical) at a dose of 5 mg/kg of body weight or vehicle was orally administered via gastric lavage sonde from day 14 to day 27. A 1:1 ratio of propylene glycol (Wako) to distilled water (Wako) was used as a diluent.

Statistical analysis

Results were expressed as mean ± SD. Significant difference between two groups of mice was analyzed using two-tailed Student *t* test. *P* values under 0.05 was considered significantly different. Overall survival was estimated via the Kaplan–Meier method using EZR software (16).

Clinical study

The single-arm, open-label, single center, phase I study following the Helsinki declaration was performed at University of Tsukuba Hospital (Tsukuba, Ibaraki, Japan) to evaluate the safety of dasatinib as a single agent in patients with relapsed or refractory AITL (UMIN000025856). Patients were enrolled between January 2017 and March 2018. The study was approved by the institutional review board at the hospital. Written informed consent was obtained from all the participants.

The 5 patients enrolled into this study were histologically diagnosed with AITL and relapsed or refractory to previous treatments. Patients must have an Eastern Cooperative Oncology Group (ECOG) performance status (PS) of 0, 1, or 2 and were required to have measurable tumors. They also needed to provide primary or relapsed tumor samples.

Dasatinib at 100 mg per body was planned to be administrated for 30 days for patient 1 and 90 days for the others (patient 2, patient 3, patient 4, and patient 5). Responses and disease status were assessed according to the Revised Response Criteria for Malignant Lymphoma (17). CT scan was performed at baseline and at days 30, 60, and 90.

Targeted sequencing

Targeted sequencing was performed for 434 genes, which are listed in Supplementary Table S3 as described previously (18) with modifications. All the exons of the selected genes were captured using a SureSelect Target Enrichment Kit (Agilent Technologies) and then massively sequenced using HiSeq2500 (Illumina). For each sample, all the sequencing reads were aligned to hg19 using Burrows-Wheeler Aligner (BWA) version 0.7.8. Candidate variants were called by Genomon pipeline (https://github.com/Genomon-Project/Genomon Pipeline). Initially, all the variants showing allele frequencies >0.02 were extracted and annotated for further consideration, if they were found in >6 reads out of >10 total reads and appeared in both the positive- and the negative-strand reads. All synonymous variants and known single-nucleotide polymorphisms (SNP) in public and our in-house databases were removed. To exclude germline variants, non-synonymous variants were excluded when the allele frequencies were higher than 0.40.

Droplet digital PCR

The G17V *RHOA* mutation was examined by droplet digital PCR (ddPCR) as described previously (19). Briefly, the PCR primer/probe mix for the G17V *RHOA* mutation purchased from BioRad was used. The probe fluorophores used for mutant and WT DNA were FAM and HEX, respectively. A 20-μL reaction mixture containing 10 μL ddPCR super mix for probe (no dUTP) × 2 (BioRad), 1 μL of 10 μmol/L primer/probe mix, and 40 ng DNA template was mixed with 70-μL droplet generation oil through microfluidics in the Droplet Generator (BioRad). Following droplet generation, the waterinoil droplets were transferred to a standard 96-well PCR plate and placed on a BioRad thermocycler for PCR amplification. Upon completion of the PCR, the plate was transferred to a Droplet Reader (BioRad). The data were initially analyzed using QuantaSoft Software (BioRad). The fluorescence threshold was set at 5,000 for FAM and 2,000 for HEX.

Results

Establishment of a mouse model for AITL treatment

Tet2$^{-/-}$G17VRHOA mice (Supplementary Figs. S1A–S1C and S2A–S2C) gradually succumbed to disease with a median survival of 48 weeks without any immunization (**Fig. 1A**). This contrasts to WT and G17VRHOA mice that remained healthy for the same time period. Twenty % of *Tet2*-null mice died of myeloid neoplasms, as reported previously (13). Histology of markedly swollen spleen and lymph nodes in Tet2$^{-/-}$G17VRHOA mice resembled that of AITL (Supplementary Fig. S3A and S3B). The lymph node and spleen architecture were totally effaced by medium-sized lymphocytes, with pale cytoplasm. The neoplastic cells were surrounded by reactive lymphocytes, eosinophils, histiocytes, and plasma cells. The spleens from tumor-bearing Tet2$^{-/-}$G17VRHOA mice contained CD4$^+$ cells as well as Gr1$^+$Mac1$^-$, Gr1$^-$Mac1$^+$, and Gr1$^+$Mac1$^+$ myeloid cells at greater proportions than WT mice (Supplementary Fig. S4A–S4C). AITL tumor cells having *TET2* and G17V *RHOA* mutations are known to express CD4, ICOS, and PD1, representative markers of T_{FH} cells (Supplementary Fig. S4C; ref. 4). Percentages of T_{FH} splenocytes estimated using flow cytometry varied from 4.84% to 80.70% in whole splenocytes in Tet2$^{-/-}$G17VRHOA mice and were significantly higher than percentages in WT mice (**Fig. 1B**; Supplementary Fig. S4A and S4B).

We previously reported that in Jurkat cells, the VAV1 hyperphosphorylation is among one of the direct consequences of G17V RHOA expression (10). Immunofluorescence staining confirmed that Vav1 phosphorylation (pVav1) was detected in CD4$^+$ and PD1$^+$ splenocytes, and PLCγ1 phosphorylation (pPLCγ1) was also detected in CD4$^+$ splenocytes of tumor-bearing Tet2$^{-/-}$G17VRHOA mice but not in those of WT mice (**Fig. 1C**). CD4$^+$ splenocytes in tumor-bearing mice showed a clonal TCR_β rearrangement pattern (Supplementary Fig. S5A–S5C; refs. 20, 21). Patients with AITL are known to exhibit symptoms by cytokine storm (22). Plasma levels of IL2, IL6, IL10, IL17A, TNF, and IFNγ were significantly higher in plasma of tumor-bearing Tet2$^{-/-}$G17VRHOA (Supplementary Fig. S6A). RNA sequencing of CD4$^+$ splenocytes obtained from tumor-bearing Tet2$^{-/-}$G17VRHOA mice indicated significant enrichment in TCR pathway genes (**Fig. 1D**) in addition to previously demonstrated genes in T-cell function and survival pathways such as IL2_STAT5, and IL6_JAK_STAT3 (Supplementary Tables S4 and S5; Supplementary Fig. S6B). T_{FH} signature genes (23) enrichment was also obvious (Supplementary Fig. S6C and S6D). All these observations indicated that Tet2$^{-/-}$G17VRHOA mice developed lymphomas exhibiting AITL-like features.

Because tumor cells did not engraft in syngenic WT mice, we used nude mice as recipients (24). By intraperitoneally injecting nude mice with single-cell suspensions prepared from swollen lymph nodes of tumor-bearing mice, we observed engraftment of H2Kb-positive cells present in peripheral blood at a frequency of >0.01%. Engraftment rate and chimerism at day 14 were both greater than values seen on day 7 (**Fig. 2A**). After the engraftment, nude mice displayed enlarged spleens (Supplementary Fig. S7A), with enlargement of follicles composed of heterogeneous cells (Supplementary Fig. S7B), as well as infiltration of mononuclear cells into liver and lungs (**Fig. 2B**). Substantial proportions (4.84% to 63.17%) of spleen and lymph node cells showed H2Kb$^+$CD4$^+$PD1$^+$ICOS$^+$, indicating T_{FH} cells of donor origin (**Fig. 2C**; Supplementary Fig. S7C). Donor CD4$^+$ splenocytes showed human *RHOA* integration and *Tet2* deletion (Supplementary Fig. S7D). Both PD1 and ICOS were expressed in significant proportions of CD4$^+$ splenocytes, pVav1 was clearly stained in both CD4$^+$ and PD1$^+$ splenocytes (**Fig. 2D**).

In summary, Tet2$^{-/-}$G17VRHOA mice developed AITL-like lymphomas and single-cell suspensions prepared from the original tumors rapidly gave rise to very similar tumors when transplanted into nude mice. This method provided us with a useful mouse model to evaluate drugs for AITL.

Dasatinib treatment prolongs overall survival of recipient mice

Dasatinib, a first-line drug for BCR-ABL–positive leukemias, inhibits multiple Src-family kinases (25). We previously reported that VAV1 hyperphosphorylation, hypothetically by Src-superfamily

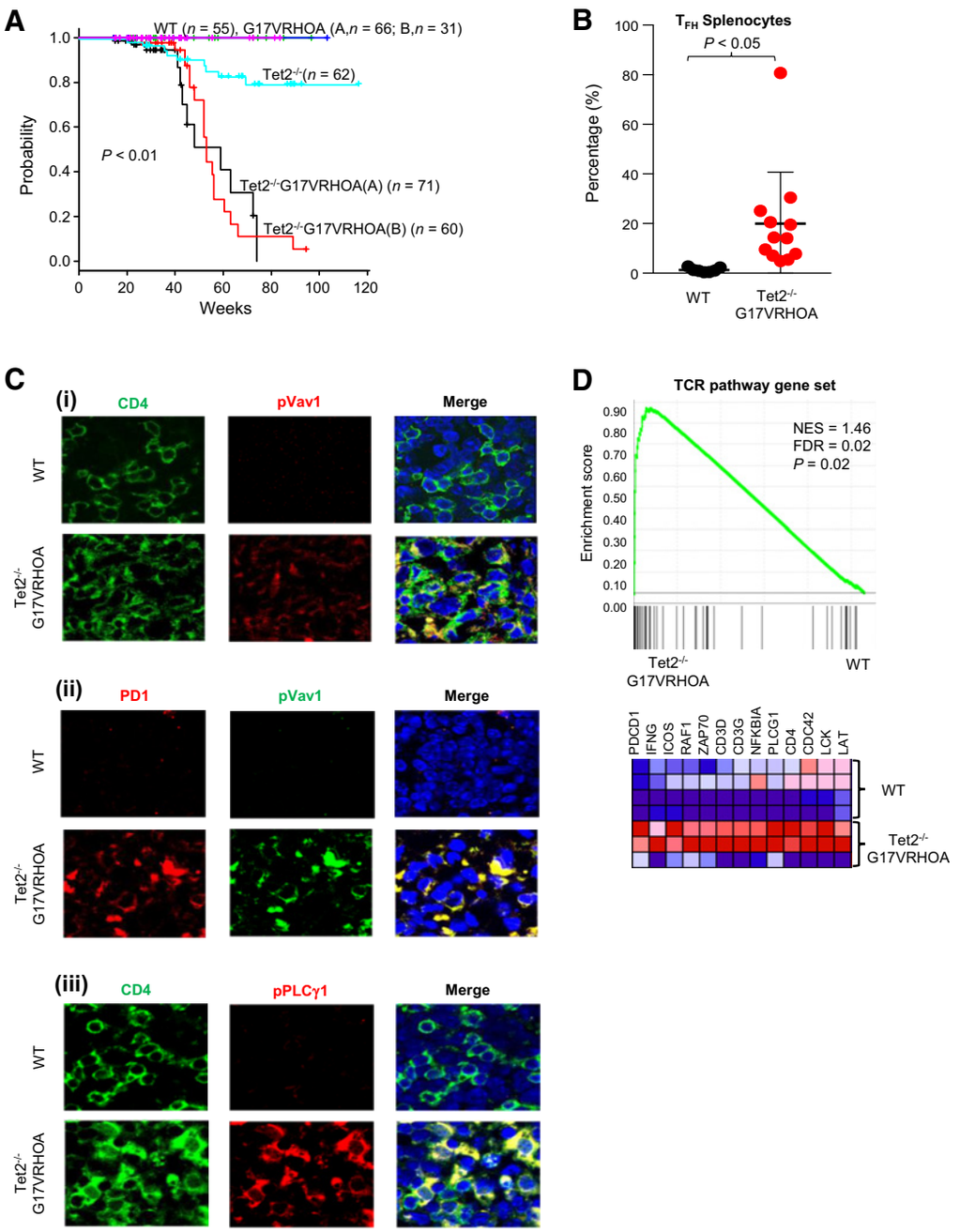

Figure 1.

Development of T_{FH}-like tumors in Tet2$^{-/-}$G17VRHOA mice. **A,** Overall survival of mice of indicated genotypes. Shown are results derived from two lines of G17VRHOA and Tet2$^{-/-}$G17VRHOA mice, as well as Tet2$^{-/-}$ and WT mice. **B,** Percentage of T_{FH} splenocytes in spleen tissues of WT ($n = 7$) and Tet2$^{-/-}$G17VRHOA ($n = 12$) mice. **C,** Immunofluorescence staining showing phosphorylated Vav1 (pVav1) in CD4$^+$ cells (**i**) and PD1$^+$ cells (**ii**), and phosphorylated PLCγ1 (pPLCγ1; **iii**) in CD4$^+$ cells in spleen tissues from mice of indicated genotypes. Pictures were taken at ×100 magnification. **D,** Enrichment of TCR pathway genes in Tet2$^{-/-}$G17VRHOA ($n = 3$) versus WT ($n = 4$) splenocytes, based on gene set enrichment analysis of RNA-sequencing data. Top, graph shows the enrichment score plot for TCR pathway gene set. Bottom, heatmap shows the expression of genes in the pathway.

kinases such as FYN and LCK, is dose-dependently inhibited by dasatinib in the Jurkat^{G17VRHOA} cell line (10). Therefore, we examined the effect of dasatinib on our AITL model nude mice. A dasatinib concentration of 10 nmol/L was required to almost completely block VAV1 phosphorylation in Jurkat^{G17VRHOA} cells (10). Others had shown that in mice a dasatinib dose of 5 mg/kg once daily was necessary to maintain plasma concentrations >10 nmol/L during the treatment period (26). Thus, we orally administered dasatinib 5 mg/kg ($n = 18$) or vehicle ($n = 18$) to recipient mice once daily from posttransplant day 14 to day 27 (**Fig. 3A**). Only 22.22% (4/18) of

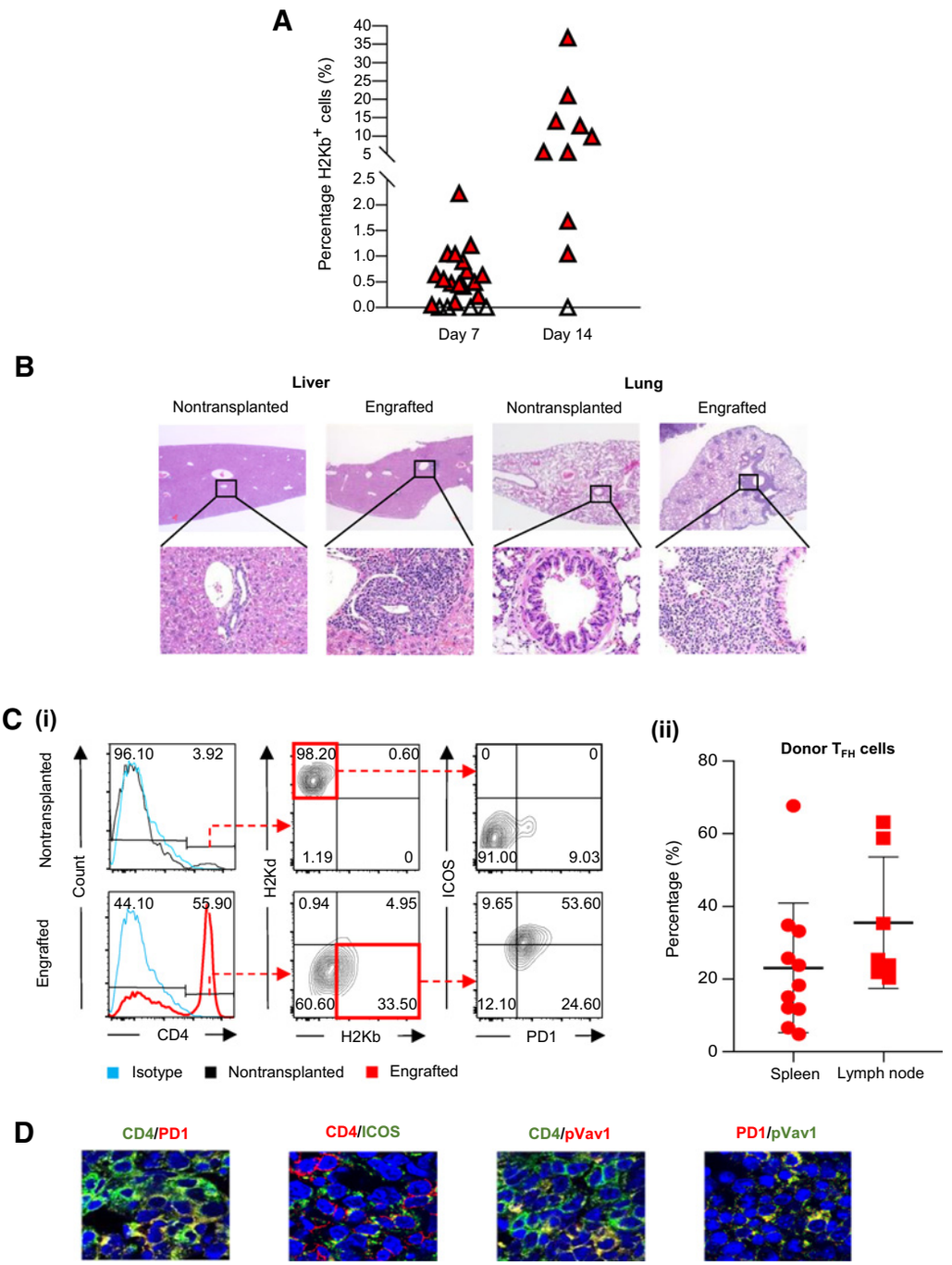

Figure 2.

Establishment of treatment model. **A,** Chimerism of donor H2Kb$^+$ cells in peripheral blood of recipient nude mice on posttransplant days 7 and 14. Red triangles, 0.01% or greater; white triangles, below 0.01%. The cut-off value used to define engraftment was determined to be 0.01%. **B,** Low (×4, top) and high (×40, bottom) magnification images showing hematoxylin and eosin staining of liver and lung specimens from indicated recipients. **C,** Characterization of donor-derived cells in spleen and lymph nodes. **i,** Flow cytometric analysis using H2Kd and H2Kb as MHC class I markers for recipients (nude) and donors (C57BL/6), respectively. **ii,** Percentages of donor-derived T_{FH} cells in spleen and lymph nodes of recipients. **D,** Staining showing the expression of the T_{FH} markers, CD4, ICOS, and PD1, and presence of phosphorylated Vav1 (pVav1) in recipient spleen cells at ×100 magnification.

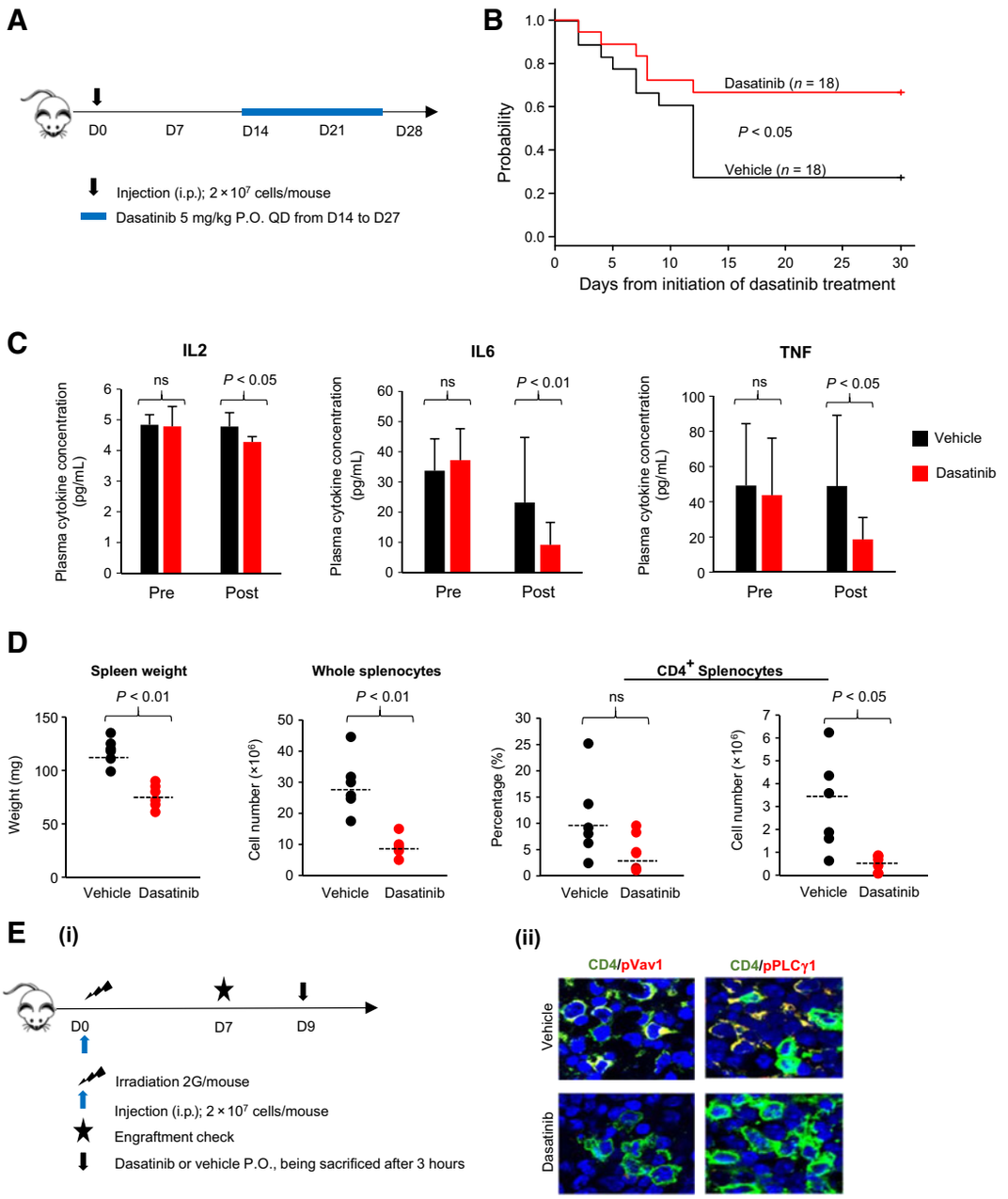

Figure 3.

Effects of dasatinib treatment on Tet2$^{-/-}$G17VRHOA tumor-bearing mice. **A,** Protocol used for vehicle or dasatinib treatment. Single-cell suspension prepared from swollen lymph nodes of Tet2$^{-/-}$G17VRHOA tumor-bearing mice was intraperitoneally injected (i.p.) into nude mice. P.O. QD, orally once a day. **B,** Survival curves for vehicle- and dasatinib-treated mice. **C,** Plasma concentrations of indicated cytokines following vehicle or dasatinib treatment. Pre, day treatment was initiated (14 days after transplant). Post, values obtained 15 days after treatment initiation. **D,** Effects of indicated treatments on spleen weight, splenocyte number, and CD4$^+$ splenocyte number. Values were obtained 6 days after treatment initiation. **E,** Dasatinib effects on phosphorylation of Vav1 (pVav1) and PLCγ1 (pPLCγ1). **i,** Protocol for sample collection after vehicle or dasatinib treatment. **ii,** Immunofluorescence staining of pVav1 and pPLCγ1 in spleen tissues at 3 hours after a single dose of vehicle or dasatinib (×100 magnification). $n = 2$, each. ns, nonsignificant.

vehicle-treated mice, while 66.67% (12/18) of dasatinib-treated mice survived at day 30 after initiation of treatment (Supplementary Table S6). Thus, dasatinib prolonged overall survival of the mice injected with Tet2$^{-/-}$G17VRHOA tumor cells ($P < 0.05$; **Fig. 3B**).

In vivo administration of dasatinib inhibits phosphorylation of Vav1 in CD4$^+$ splenocytes

We evaluated plasma cytokine concentrations in dasatinib- or vehicle-treated mice on the day following completion of treatment using a nonirradiation protocol (at posttransplant day 28; **Fig. 3C**).

Plasma concentrations of IL2, IL6, and TNF were significantly decreased in dasatinib- versus vehicle-treated mice [IL2, 4.28 ± 0.18 vs. 4.85 ± 0.66; IL6, 9.17 ± 7.42 vs. 25.64 ± 7.97; TNF, 18.68 ± 12.37 vs. 53.77 ± 30.92 ($P < 0.05$)]. Concentrations of IL10, IL17A, and IFNγ were comparable between both groups (Supplementary Fig. S8A).

We also evaluated the effect of dasatinib on spleen cells. On posttransplant day 14, we initiated treatment with dasatinib or vehicle of recipients whose engraftment had been confirmed ($n = 6$, each). Mice were then sacrificed after a 6-day treatment period. At the end of that period, dasatinib-treated mice showed lower spleen weight and a smaller number of splenocytes than did vehicle-treated mice ($P < 0.01$; **Fig. 3D**). Proportions of $CD4^+$ splenocytes in dasatinib-treated mice also tended to be lower. Moreover, the absolute number of $CD4^+$ splenocytes in dasatinib-treated mice was significantly smaller than that seen in vehicle-treated mice ($P < 0.05$; **Fig. 3D**).

To directly measure dasatinib effects on Vav1 and PLCγ1 phosphorylation *in vivo*, we performed immunofluorescence analysis for pVav1, pPLCγ1, and CD4 in spleen tissues from dasatinib- and vehicle-treated mice. In mice, dasatinib is reported to time-dependently inhibit BCR-ABL phosphorylation in transplanted K562 chronic myelogenous leukemia cells, an inhibition clearly apparent by 3 hours after administration of a single oral dose (27). Thus, on posttransplant day 9, we evaluated pVav1 and pPLCγ1 in $CD4^+$ splenocytes 3 hours after a single oral dose of dasatinib or vehicle [**Fig. 3E** (**i**)]. The approximate frequencies of $CD4^+$ splenocytes was comparable in both groups; however, the number of $CD4^+$ splenocytes displaying pVav1 and pPLCγ1 decreased in dasatinib- versus vehicle-treated mice [**Fig. 3E** (**ii**)]. We also examined the number of pVav1-positive splenocytes on day 6 of daily treatment with dasatinib and found that it was significantly decreased in dasatinib-treated mice (Supplementary Fig. S8B).

We conclude that dasatinib treatment inhibits Vav1 and PLCγ1 phosphorylation and subsequent activation of TCR signaling, improving the survival of AITL model mice.

Patients with relapsed/refractory AITL respond to dasatinib

On the basis of our *in vitro* and *in vivo* observations, we tested dasatinib in a clinical trial. The study design was approved by the institutional review board of University of Tsukuba Hospital (Tsukuba, Ibaraki, Japan). We enrolled 5 patients (one male, four female; 51–72 years old; median, 65 years old) previously diagnosed with and treated for AITL and obtained written informed consent from all. All patients had a relapsed/refractory disease after prior chemotherapies (for details see **Table 1**). The median number of prior chemotherapies was 2 (range: 1–5). Two patients (1 and 2) were refractory to the latest chemotherapies. One (patient 3) relapsed after autologous transplantation. The median PS was 1 (range: 0–2).

Dasatinib treatment (100 mg) was initiated and administered once daily for 10–70 days (median, 58 days). Patient 2 withdrew consent, and analysis of that individual was discontinued on day 10. Dasatinib treatment of the remaining four continued until day 54 or later, when responses were evaluated. A partial response (PR) was achieved in all remaining patients (1, 3, 4, and 5) after 30 days of dasatinib treatment, based on commonly used response criteria (Supplementary Results and Supplementary Fig. S9A and S9B; ref. 17). The response at trial discontinuation was PR for patients 1 and 5 and progressive disease in patients 3 and 4 (**Fig. 4A**). Adverse events most attributable to disease exacerbation, or those potentially to drug reactions, were shown in **Table 2**. Grade 3/4 adverse drug reactions were observed in patient 5. There were no previously undocumented safety concerns (28).

Targeted sequencing was performed in five tumor samples (Supplementary Table S7) using a panel of 434 genes (Supplementary Table S3). Overall, we identified 33 candidate mutations, including 22 nonsilent single-nucleotide variants, two nonsense mutations, three frameshift deletions, two frameshift insertions, two nonframeshift deletions, one nonframeshift insertion, and one tandem duplication (**Fig. 4B**; Supplementary Table S8). Two different *TET2* mutations were found in each of the 4 samples (patients 1, 2, 4, and 5). G17V *RHOA* mutations were found in 2 samples (patients 3 and 4; **Fig. 4B**; Supplementary Fig. S10A and S10B; the one in patient 3 was found only by ddPCR assay). *VAV1* mutations were identified in two samples patients 2 and 5; **Fig. 4B**; Supplementary Table S8; Supplementary

Table 1. Characteristics of patients enrolled in the study.

Patient	Disease	Age	Sex	PS	Number of prior regimens	Prior chemotherapies		Prior autologous transplantation
						CTx	Response	
PAT1	AITL	51	F	1	4	CHOP	PD	No
						High-dose MA	PD	
						GCD	PD	
						Mogamulizumab	PD	
PAT2	AITL	68	M	1	2	R-CHOP[a]	CR	No
						DeVIC	PD	
PAT3	AITL	65	F	0	2	CHOP	PR	Yes
						CHASE	CR	
PAT4	AITL	72	F	2	5	CHOP	CR	No
						CarboESHAP	CR	
						Romidepsine	Unknown	
						Prednisone	PD	
						High-dose Dex	PR	
PAT5	AITL	63	F	0	1	CHOP	CR	No

Abbreviations: CTx, chemotherapy; CHOP, cyclophosphamide, doxorubicin, vincristine, and prednisone; MA, methotrexate and cytarabine; GCD, gemcitabine, carboplatin, and dexamethasone; R-CHOP, rituximab, CHOP; DeVIC, dexamethasone, carboplatin, etoposide, ifosphamide; CHASE, cyclophosphamide, cytarabine, etoposide, dexamethasone; CarboESHAP, carboplatin, etoposide, cytarabine, methylprednisone; Dex, dexamethasone; PD, progressive disease; CR, complete response; PR, partial response..

[a]R-CHOP was performed because the patient's tumor cells aberrantly expressed CD20 at diagnosis; CD20 expression was not confirmed at relapse.

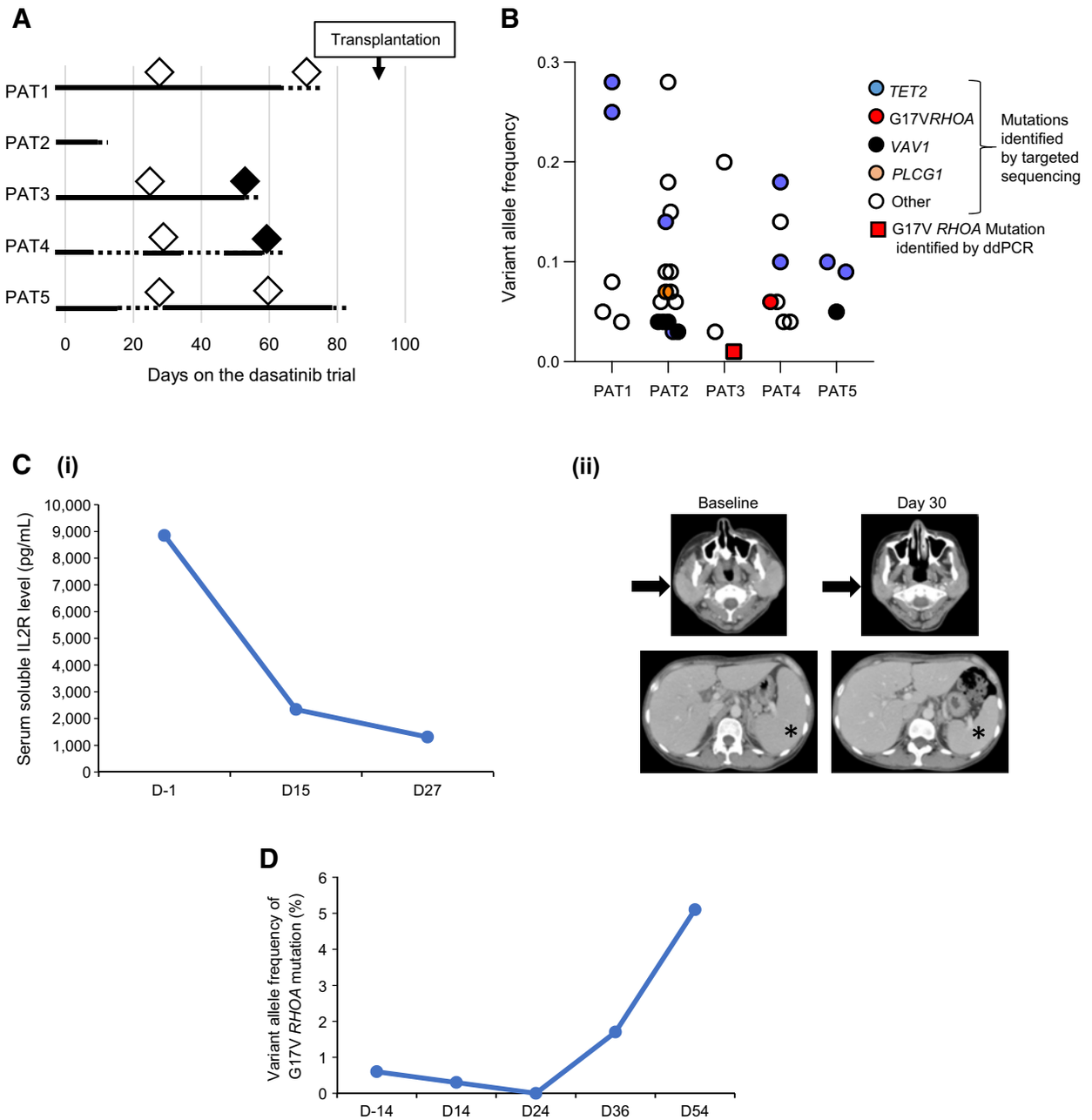

Figure 4.

Clinical trial of dasatinib for patients with relapsed/refractory AITL. **A,** Time course of dasatinib treatment for each patient (PAT). Open diamond, partial response; closed diamond, relapse; dotted line, dasatinib interruption. **B,** Mutation profiles of biopsied samples from patients 1–5. **C,** Response to dasatinib treatment in patient 1. **i,** Serum soluble IL2 receptor levels on days (D) 1, 15, and 27 of dasatinib treatment. **ii,** CT scan performed before (Baseline) and 30 days after initiation of dasatinib treatment. Arrow, parotid glands. Asterisk, spleen. **D,** Detection of the G17V *RHOA* mutation in serum cell-free DNA from patient 3 examined by ddPCR. VAFs of the G17V *RHOA* mutation on days (D) 14, 14, 24, 36, and 54 are shown.

Fig. S11A and S11B). One tandem duplication mutation involving the *VAV1* locus was identified by manual inspection on the integrative genome viewer in patient 5 (Supplementary Fig. S12A–S12D).

In patient 1, serum levels of soluble IL2 receptor decreased at 2 weeks and later from the dasatinib initiation [**Fig. 4C** (**i**)]. A CT scan on day 30 met the criteria of PR [**Fig. 4C** (**ii**)]. Dasatinib was discontinued on day 70 before allogenic peripheral blood stem cell transplantation, which was performed on day 86 after the treatment initiation (**Fig. 4A**).

In patient 3, the G17V *RHOA* mutation was detected in serum cell-free DNA with a variant allele frequency (VAF) of 0.60% at the time of relapse. The VAF was decreased below the detection level on day 24,

Table 2. Adverse events seen in dasatinib-treated patients.

Patient	Adverse reaction	Grade
PAT1	Platelet count decreased	1
	Fibrinogen decreased	2
	Anemia	3
	Fever	1
	Diarrhea	2
PAT2	Pharyngolaryngeal pain	3
	Fever	2
PAT3	Platelet count decreased	1
	Pleural effusion	3
	Deterioration of original disease	3
PAT4	Anemia	3
	Electrocardiogram QT corrected interval prolonged	1
	Platelet count decreased	1
	Fever	1
	Pleural effusion	1
	Ascites	1
	Deterioration of original disease	5
PAT5	Electrocardiogram QT corrected interval prolonged	1
	Cardiac disorders (coronary artery disease)	3
	Neuralgia	3

but became detectable on day 36 with VAF of 1.70% and increased later, corresponding to the clinical course (**Fig. 4D**).

Discussion

Here, we report that *Tet2* loss paired with expression of the G17V RHOA mutant in mice led to development of AITL-like lymphomas. Dasatinib treatment prolonged overall survival of those mice and was also effective in treating patients with relapsed/refractory AITL.

Three models of G17V RHOA–expressing mice were previously reported: adoptive transfer of retrovirally transduced T cells by Zang and colleagues (29), G17V knock-in by Cortes and colleagues (30), and transgenic G17V expression by Ng and colleagues (31). In our model, transgenic human G17V RHOA was expressed under control of the human *CD2* promoter. Although Ng and colleagues (31) found developed autoimmune disease and Cortes and colleagues (30) showed induction of T_{FH} cell specification with the similar models, we did not notice major phenotypes nor did Zang and colleagues. The differences in the phenotypes was presumably attributed to the difference of the experimental systems.

Like us, all three groups cited above also established G17V RHOA expression in T cells on a *Tet2*$^{-/-}$ background to model human AITL (5, 6, 18). Zang and colleagues (29) adoptively transferred T cells overexpressing G17V RHOA into mice in which *Tet2* was disrupted in all tissues. These mice developed lethal autoimmune disease while tumor development was not observed. Cortes and colleagues (30) transplanted G17V RHOA knock-in;*Tet2*$^{-/-}$ (CD4-CreER^{T2}) bone marrow progenitors into irradiated mice then immunized animals with sheep red blood cells; their mice developed AITL-like lymphomas 175 days later. Moreover, they reported that treatment with either anti–ICOS-ligand–blocking antibody or a PI3K δ/γ inhibitor (duvesilib) inhibited *in vivo* tumor proliferation in their model. Finally, Ng and colleagues (31) generated transgenic CD4-G17V RHOA;*Tet2*$^{-/-}$ (VAV-Cre);OT-II TCR mice and immunized them with NP-40-Ova; these mice developed AITL-like lymphomas 270 days later. They also reported that treatment with an mTORC1 inhibitor (everolimus) effectively prolonged overall survival of Nod-scid Il2rγ$^{-/-}$ mice transplanted with G17VRHOA;*Tet2*$^{-/-}$ (VAV-Cre);OT-II TCR lymphoma cells.

As reported here, our original mice developed AITL-like lymphomas after 336 days without immunization and the tumor recipients responded positively to dasatinib treatment. Among dasatinib targets are LYN and FYN, the two key tyrosine kinases in the TCR pathway. Moreover, in our treatment model we observed inhibition of Vav1 phosphorylation in spleen tissue following dasatinib. Importantly, using our AITL model in the recipient nude mice, we were able to demonstrate Vav1 dephosphorylation *in vivo*.

Among the 4 patients that responded to dasatinib in the clinical part of this study, two harbored G17V *RHOA* mutations and one exhibited *VAV1* mutations. These 3 patients' responses support our hypothesis that dasatinib is a candidate drug to treat tumors harboring G17V *RHOA* mutations. The one remaining patient that completed the trial and showed a positive response to dasatinib did not exhibit *RHOA*-, *VAV1*-, or TCR pathway–related mutations, although the patient harbored two *TET2* mutations. It is also possible that this patient carries mutations in FYN/LCK–dependent TCR pathway genes not incorporated in our sequencing panel. Alternatively, dasatinib may inhibit pathways other than TCR (32). This patient's response suggests that G17V *RHOA* or *VAV1* mutations do not necessarily predict dasatinib efficacy in AITL. Meanwhile, a phase I/II study of dasatinib as treatment for relapse/refractory non-Hodgkin lymphomas reported a patient with AITL achieving a PR, in agreement with our study (33).

Recently, many new drugs have been introduced as promising therapeutics for PTCL including AITL (34–36). However, no monotherapies yet satisfactorily improve overall survival in relapsed/refractory cases. Our work suggests that targeting the TCR pathway should be considered in developing AITL treatment strategies.

Disclosure of Potential Conflicts of Interest

M. Sakata-Yanagimoto has received speakers bureau honoraria from Bristol-Myers Squibb. S. Chiba is a paid consultant for Daiichi-Sankyo, Sorrento Therapeutics and reports receiving other commercial research support from Astellas, Ono Pharmaceutical Co., Kyowa Kirin, Sanofi, Takeda Pharmaceutical Co., and Chugai Pharmaceutical Co. and has received speakers bureau honoraria from Bristol-Myers Squibb. No potential conflicts of interest were disclosed by the other authors.

Authors' Contributions

Conception and design: T.B. Nguyen, M. Sakata-Yanagimoto, S. Chiba
Development of methodology: T.B. Nguyen, M. Fujisawa, K. Hashimoto, K. Fukumoto
Acquisition of data (provided animals, acquired and managed patients, provided facilities, etc.): M. Sakata-Yanagimoto, M. Fujisawa, Y. Kiyoki, K. Ishitsuka, H. Momose, S. Sukegawa, A. Shinagawa, T. Suyama, Y. Sato, H. Nishikii, N. Obara, M. Kusakabe, S. Ogawa, K. Ohshima
Analysis and interpretation of data (e.g., statistical analysis, biostatistics, computational analysis): T.B. Nguyen, M. Sakata-Yanagimoto, S.T. Nuhat, H. Miyoshi, Y. Nannya, K. Fukumoto, S. Yanagimoto
Writing, review, and/or revision of the manuscript: T.B. Nguyen, M. Sakata-Yanagimoto, S. Chiba
Study supervision: M. Sakata-Yanagimoto, S. Chiba
Others (provided material): O.A. Bernard

Acknowledgments

The authors thank Dr. Elise Lamar at www.eliselamar.com and Associate Professor Thomas Mayers at Medical English Communications Center, University of Tsukuba (Tsukuba, Ibaraki, Japan), for their editorial assistance. This work was supported by Grants-in-Aid for Scientific Research (KAKENHI: 18K16077 to T.B. Nguyen; 18H02834 to M. Sakata-Yanagimoto; 16H02660 and 19H03684 to S. Chiba) from the Ministry of Education, Culture, Sports, and Science of Japan; AMED under

grant numbers JP17ck0106365h (to M. Sakata-Yanagimoto) and JP16cm0106505h (to S. Chiba); the Japan Research Foundation for Clinical Pharmacology, MSD Life Science Foundation, Takeda Science Foundation, Leukemia Research Fund, Kobayashi Foundation for Cancer Research, and Suzuken Memorial Foundation (to M. Sakata-Yanagimoto); and the Uehara Memorial Foundation (to S. Chiba). The clinical study was supported by the Grant for Implementation of Advanced Medicine in University of Tsukuba Hospital (Tsukuba, Ibaraki, Japan).

The costs of publication of this article were defrayed in part by the payment of page charges. This article must therefore be hereby marked *advertisement* in accordance with 18 U.S.C. Section 1734 solely to indicate this fact.

Received September 5, 2019; revised December 25, 2019; accepted February 25, 2020; published first February 27, 2020.

References

1. Vose J, Armitage J, Weisenburger D. International peripheral T-cell and natural killer/T-cell lymphoma study: pathology findings and clinical outcomes. J Clin Oncol 2008;26:4124–30.
2. Xu B, Liu P. No survival improvement for patients with angioimmunoblastic T-cell lymphoma over the past two decades: a population-based study of 1207 cases. PLoS One 2014;9:e92585.
3. Bellei M, Foss FM, Shustov AR, Horwitz SM, Marcheselli L, Kim WS, et al. The outcome of peripheral T-cell lymphoma patients failing first-line therapy: a report from the prospective, International T-Cell Project. Haematologica 2018; 103:1191–7.
4. Swerdlow SH, Campo E, Harris NL, Jaffe ES, Pileri SA, Stein H, et al. WHO classification of tumors of haematopoietic and lymphoid tissues. Lyon, France: International Agency for Research on Cancer; 2017. p 407–12.
5. Sakata-Yanagimoto M, Enami T, Yoshida K, Shiraishi Y, Ishii R, Miyake Y, et al. Somatic RHOA mutation in angioimmunoblastic T cell lymphoma. Nat Genet 2014;46:171–5.
6. Palomero T, Couronné L, Khiabanian H, Kim MY, Ambesi-Impiombato A, Perez-Garcia A, et al. Recurrent mutations in epigenetic regulators, RHOA and FYN kinase in peripheral T cell lymphomas. Nat Genet 2014;46:166–70.
7. Yoo HY, Sung MK, Lee SH, Kim S, Lee H, Park S, et al. A recurrent inactivating mutation in RHOA GTPase in angioimmunoblastic T cell lymphoma. Nat Genet 2014;46:371–5.
8. Lemonnier F, Couronné L, Parrens M, Jaïs JP, Travert M, Lamant L, et al. Recurrent TET2 mutations in peripheral T-cell lymphomas correlate with TFH-like features and adverse clinical parameters. Blood 2012;120:1466–9.
9. Chiba S, Enami T, Ogawa S, Sakata-Yanagimoto M. G17V RHOA: genetic evidence of GTP-unbound RHOA playing a role in tumorigenesis in T cells. Small GTPases 2015;6:100–3.
10. Fujisawa M, Sakata-Yanagimoto M, Nishizawa S, Komori D, Gershon P, Kiryu M, et al. Activation of RHOA-VAV1 signaling in angioimmunoblastic T-cell lymphoma. Leukemia 2018;32:694–702.
11. Saveliev A, Vanes L, Ksionda O, Rapley J, Smerdon SJ, Rittinger K, et al. Function of the nucleotide exchange activity of vav1 in T cell development and activation. Sci Signal 2009;2:ra83.
12. Zhumabekov T, Corbella P, Tolaini M, Kioussis D. Improved version of a human CD2 minigene based vector for T cell-specific expression in transgenic mice. J Immunol Methods 1995;185:133–40.
13. Quivoron C, Couronné L, Della Valle V, Lopez CK, Plo I, Wagner-Ballon O, et al. TET2 inactivation results in pleiotropic hematopoietic abnormalities in mouse and is a recurrent event during human lymphomagenesis. Cancer Cell 2011;20: 25–38.
14. Kühn R, Schwenk F, Aguet M, Rajewsky K. Inducible gene targeting in mice. Science 1995;269:1427–9.
15. Subramanian A, Tamayo P, Mootha VK, Mukherjee S, Ebert BL, Gillette MA, et al. Gene set enrichment analysis: a knowledge-based approach for interpreting genome-wide expression profiles. Proc Natl Acad Sci U S A 2005;102:15545–50.
16. Kanda Y. Investigation of the freely available easy-to-use software 'EZR' for medical statistics. Bone Marrow Transplant 2013;48:452–8.
17. Cheson BD, Pfistner B, Juweid ME, Gascoyne RD, Specht L, Horning SJ, et al. Revised response criteria for malignant lymphoma. J Clin Oncol 2007;25:579–86.
18. Nguyen TB, Sakata-Yanagimoto M, Asabe Y, Matsubara D, Kano J, Yoshida K, et al. Identification of cell-type-specific mutations in nodal T-cell lymphomas. Blood Cancer J 2017;7:e516.
19. Tanzima Nuhat S, Sakata-Yanagimoto M, Komori D, Hattori K, Suehara Y, Fukumoto K, et al. Droplet digital polymerase chain reaction assay and peptide nucleic acid-locked nucleic acid clamp method for RHOA mutation detection in angioimmunoblastic T-cell lymphoma. Cancer Sci 2018;109:1682–9.
20. Giudicelli V, Brochet X, Lefranc MP. IMGT/V-QUEST: IMGT standardized analysis of the immunoglobulin (IG) and T cell receptor (TR) nucleotide sequences. Cold Spring Harb Protoc 2011;2011:695–715.
21. Brochet X, Lefranc MP, Giudicelli V. IMGT/V-QUEST: the highly customized and integrated system for IG and TR standardized V-J and V-D-J sequence analysis. Nucleic Acids Res 2008;36:W503–8.
22. Yi JH, Ryu KJ, Ko YH, Kim WS, Kim SJ. Profiles of serum cytokines and their clinical implications in patients with peripheral T-cell lymphoma. Cytokine 2019;113:371–9.
23. Chtanova T, Tangye SG, Newton R, Frank N, Hodge MR, Rolph MS, et al. T follicular helper cells express a distinctive transcriptional profile, reflecting their role as non-Th1/Th2 effector cells that provide help for B cells. J Immunol 2004; 173:68–78.
24. Morito N, Yoh K, Fujioka Y, Nakano T, Shimohata H, Hashimoto Y, et al. Overexpression of c-Maf contributes to T-cell lymphoma in both mice and human. Cancer Res 2006;66:812–9.
25. Lombardo LJ, Lee FY, Chen P, Norris D, Barrish JC, Behnia K, et al. Discovery of N-(2-chloro-6-methyl- phenyl)-2-(6-(4-(2-hydroxyethyl)- piperazin-1-yl)-2-methylpyrimidin-4-ylamino)thiazole-5-carboxamide (BMS-354825), a dual Src/Abl kinase inhibitor with potent antitumor activity in preclinical assays. J Med Chem 2004;47:6658–61.
26. Kamath AV, Wang J, Lee FY, Marathe PH. Preclinical pharmacokinetics and in vitro metabolism of dasatinib (BMS-354825): a potent oral multi-targeted kinase inhibitor against SRC and BCR-ABL. Cancer Chemother Pharmacol 2008;61:365–76.
27. Luo FR, Yang Z, Camuso A, Smykla R, McGlinchey K, Fager K, et al. Dasatinib (BMS-354825) pharmacokinetics and pharmacodynamic biomarkers in animal models predict optimal clinical exposure. Clin Cancer Res 2006;12:7180–6.
28. Kantarjian H, Shah NP, Hochhaus A, Cortes J, Shah S, Ayala M, et al. Dasatinib versus imatinib in newly diagnosed chronic-phase chronic myeloid leukemia. N Engl J Med 2010;362:2260–70.
29. Zang S, Li J, Yang H, Zeng H, Han W, Zhang J, et al. Mutations in 5-methylcytosine oxidase TET2 and RhoA cooperatively disrupt T cell homeostasis. J Clin Invest 2017;127:2998–3012.
30. Cortes JR, Ambesi-Impiombato A, Couronne L, Quinn SA, Kim CS, da Silva Almeida AC, et al. RHOA G17V induces T follicular helper cell specification and promotes lymphomagenesis. Cancer Cell 2018;33:259–73.
31. Ng SY, Brown L, Stevenson K, deSouza T, Aster JC, Louissaint A, et al. RhoA G17V is sufficient to induce autoimmunity and promotes T-cell lymphomagenesis in mice. Blood 2018;132:935–47.
32. Das J, Chen P, Norris D, Padmanabha R, Lin J, Moquin RV, et al. 2-aminothiazole as a novel kinase inhibitor template. Structure-activity relationship studies toward the discovery of N-(2-chloro-6-methylphenyl)-2-[[6-[4-(2-hydroxyethyl)-1-piperazinyl)]-2-methyl-4-pyrimidinyl]amino)]-1,3-thiazole-5-carboxamide (dasatinib, BMS-354825) as a potent pan-Src kinase inhibitor. J Med Chem 2006;49:6819–32.
33. Umakanthan JM, Iqbal J, Batlevi CL, Bouska A, Smith LM, Shostrom V, et al. Phase I/II study of dasatinib and exploratory genomic analysis in relapsed or refractory non-Hodgkin lymphoma. Br J Haematol 2019;184:744–52.
34. Fujisawa M, Chiba S, Sakata-Yanagimoto M. Recent progress in the understanding of angioimmunoblastic T-cell lymphoma. J Clin Exp Hematop 2017;57: 109–19.
35. Laribi K, Alani M, Truong C, Baugier de Materre A. Recent advances in the treatment of peripheral T-cell lymphoma. Oncologist 2018;23:1039–53.
36. Ma H, Davarifar A, Amengual JE. The future of combination therapies for peripheral T cell lymphoma (PTCL). Curr Hematol Malig Rep 2018;13:13–24.